Journal of Engineering Science and Technology Review 11 (1) (2018) 138 - 145

Research Article

JOURNAL OF
Engineering Science and Technology Review

www.jestr.org

Three Dimensional CFD Simulations of A Wind Turbine Blade Section; Validation

Patrick Irungu Muiruri* and Oboetswe Seraga Motsamai

Department of Mechanical, Faculty of Engineering and technology, University of Botswana, P.O. Box 0061, Gaborone, Botswana.

Received 1 December 2017; Accepted 15 February 2018

Abstract

The purpose of present study is to approve use of ANSYS software as a tool for wind turbine simulations. Based on workbench platform designmodeler, mechanical mesh and fluent components, the study attempts to reproduce experimental measurements performed on standstill outboard MEXICO blade section in the low speed low turbulence (LTT), a facility at Delft University of Technology. The outboard MEXICO blade section geometry same as the one used in experiments is adopted for numerical simulations. Three set of angle of attack are taken as variable with inlet velocity hold at 35 m/s and fluid flow viscosity at $1.462kgms^{-2}$ in every simulation. Steady state pressure based solver is utilized to solve continuity and momentum Navier-Stoke equations with $k-\omega$ SST turbulent model taken as closure. Pressure and velocity are decoupled via SIMPLE algorithm and discretization scheme specified to second order upwind for momentum, turbulent kinetic energy and dissipation rate, while pressure interpolation scheme settled to second order. Computed pressure coefficient around selected airfoil sections is compared to experiment measurements which include; RISOE_121 at 60%R and NACA64418 at 92%R. Comparison shows good agreement between the CFD simulation and experiment results, but slight variation is observed at around RISOE_121 airfoil.

Keywords:CFD simulations; Coefficient of pressure; Comparison; Experiment measurement; MEXICO Blade.

1. Introduction

Use of fossil fuels as a source of power produces greenhouse gases to the atmosphere, which causes climate change. As a result, the global warming which is one of the climate change effects, is negatively affecting human life. At the same time, the world energy demand is rapidly increasing putting the world in huge global energy crisis [1]. In search for solution, mitigation of greenhouse gas emissions can be achieved through exploration of untapped renewable sources such as; wind, biogas, solar and geothermal. From previous research [2-4], they are found potential in providing an alternative to fossil fuels, thereby reducing greenhouse gas emissions and increase energy supply. These sources are clean, free available, inexpensive and widely distributed worldwide. Based on assessment for sustainability indicators in global view, wind technology is ranked the most sustainable among others renewable technologies [5]. All indicators used in evaluation, were assumed to have equal importance for sustainability development and they include; costs of generated electricity, greenhouse gas emissions during full life cycle, availability of renewable sources, efficiency of energy conversion, land requirements, water consumption and social impact [5]. Wind energy continues to enjoy attention among others renewable source in addition to fact that it is the most clean green energy [6], despite occurring irregularly. Motivation of the present study is founded by aforementioned facts about wind energy.

Wind is transformed to useful energy via two stages namely; primary and secondary stages [7]. In primary stage, the blades extract kinetic energy from the moving air and transform it into torque load at the hub axis. The obtained mechanical energy is transmitted and converted into electricity in the generator via transmission systems in secondary stage. Most of investigations carried on rotor tend to improve aerodynamics of the blades in order to increase performance and efficiency of wind turbines [7, 8]. The approaches of these studies include experimental, analytical and numerical methods. The experimental methods are reliable but limited to model size and expensive. Despite these methods being reliable, the accuracy of data interpolation from small scaled model to large scale model is not guarantee for making rational decision. Instead, computational method can resolve aforementioned gap since it has capacity to simulate full scale model and probe area of interest precisely.

The Blade Element Momentum (BEM) theory is extensively used in the industries due to less computation time, simplicity and presence of most of physics features representing rotor aerodynamics. Aerodynamic performance and optimization of wind turbines has been widely investigated using this BEM theory as well as Genetic Algorithms (GA) and XFOIL software [9]. In real situation, wind turbines are subjected to harsh atmospheric turbulence, wind shear from ground effect, wind direction that change in time and space and effects from wake of neighbouring wind turbines [7]. The BEM simulations are, therefore, inadequately account for aforementioned conditions, based on the fact that, BEM simulations are implemented based on input of empirical assumptions. Instead, CFD tool can provide a reliable alternative to simulate aerodynamic behaviour for wind turbine development technology.

With significant improvement of computer architecture and numerical algorithms, CFD methods are favourable for

*E-mail address: pmuiruri@jkuat.ac.ke
ISSN: 1791-2377 © 2018 Eastern Macedonia and Thrace Institute of Technology. All rights reserved.
doi:10.25103/jestr.111.16

the design of wind turbines as attributed to drastically reduction of computation time [10]. Three-dimensional (3D) simulation has authority to specify real operating boundary conditions and probes quantities of interest at any given location [8]. But, CFD simulations require validation from experimental data, in order to justify their fidelity. Today, MEXICO project [11] under collaboration and partnership of 10 institutes from 6 countries in the MEXNEXT framework provides a wide range of experimental measurement data set for purposes of validating various aerodynamic numerical models ranging from BEM to CFD [12].

Numerous CFD simulations using various solvers and turbulence models have been successfully compared with MEXICO experimental data in various studies [10, 13-16]. Carrion et al [13] summarized CFD aerodynamic analysis studies ranging from 2D simulations to 3D simulations. In the study of Schepers et al. [17], wind tunnel effects reported to have shown little discrepancy on computation, even though the authors suggest for use of exact wind tunnel geometries. Réthoré et al. [18], compared MEXICO experiments with CFD simulation using OpenFoam by modelling exact geometry of wind tunnel and wind turbine rotor. A non-rotating MEXICO blade has been investigated through experiments and OpenFoam simulations [16]. Several uncertainties that occur due to rotational effects as well as complex flow over rotating blade are eliminated by adopting non-rotating blade.

The present study seeks to validate CFD results with experimental measurements performed by Zhang et al. [16]. Methodology used in this study, uses ANSYS workbench platform to model, mesh and solve numerical problem. Designmodeler is used to create geometry, workbench mesh to generate mesh elements and FLUENT solver V172 to perform specified simulations of the blade. The study extends to investigate influence of different turbulent models for Reynolds Average Navier-Stoke equations (RANS) closure. The obtained results are then compared with experimental measurements for different airfoil sections span-wise that include 60%R and 92%R at different angle of attacks ($\alpha = 8^0$, $\alpha = 15^0$ and $\alpha = 19^0$).

2. Numerical methodology

Numerical study is completed using steps illustrated on flowchart in Fig.1 for every chosen simulation.

First, geometry of the blade section and fluid domain are modelled in ANSYS designmodeler to exact measurement of wind tunnel test section. In present study, we consider a blade section for a length measured starting from 53%R to tip. The origin design of MEXICO turbine blade has a rotor radius equal to 2.25m. The blade is made of three different types of airfoil which are distributed span-wise as shown in Fig. 2.

Likewise Fig. 3 shows relationship of twist angles and chord length distribution along the span for the blade section selected in the present study.

For fluid domain shown in Fig. 4, a cylindrical enclosing the blade is inserted in the main fluid domain to facilitate adjustment of angle of attack (α) and refinement of mesh around the blade to capture boundary layers on blade surfaces. The red stripes on the blade indicate specified computational positions of interest. Fig. 4 also displays boundary geometry.

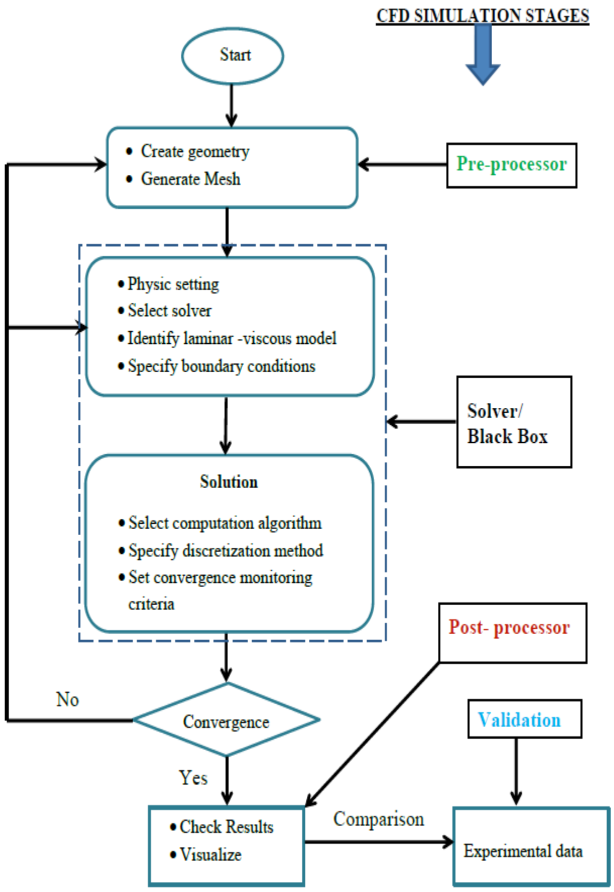

Fig. 1. CFD numerical methodology flow chart

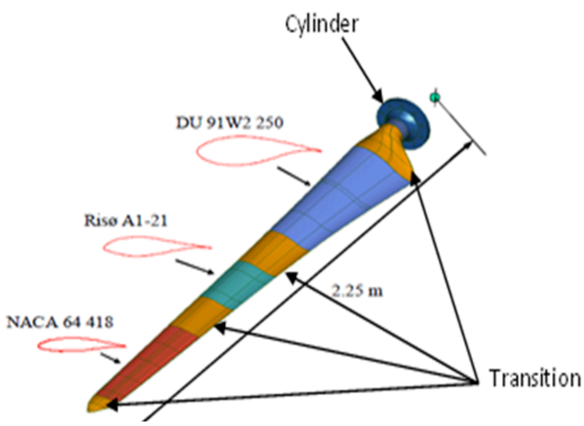

Fig. 2. MEXICO balede layout

The next step in pre-processor involves generation of meshing grids. The accuracy of CFD simulation results depend on quality of generated mesh elements. However, due to computation time requirements and capacity of computer memory to perform simulations, compromise is drawn between computation time, mesh grid density and accuracy. For high precision results to be obtained, a high performance of the computer is required for fluent simulation. In this study, a HP desktop computer installed with 64 bit Operating System (OS), Intel(R) Core (TM) i5-3570 CPU @ 3.40GHz 3.40GHz processor and 12.0GB RAM has been used.

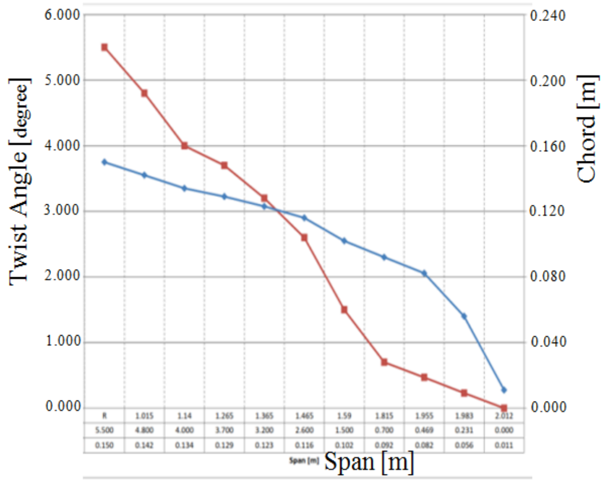

Fig. 3 Relationship between twist angle and chord distribution

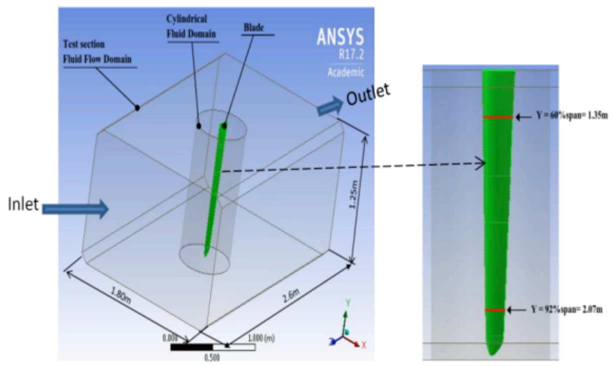

Fig. 4. Fluid domain geometry and model alignment in domain

Local mesh size function was specified to proximity and curvature with medium relevance centre. In order to refine mesh grids, curvature normal to angle was changed to 9^0. The size of blade surface mesh was specified to be 0.0025m, bounded with twenty smooth transition inflation layers with growth rate left as default of 1.2. The inflation layers are purposely applied in attempt to resolve boundary layers near the wall surfaces of the blade. Mesh interface was created between cylindrical boundary and main fluid domain boundary for smooth transition of flow in between two domains boundary. With specified setting, the total number of nodes and elements generated slightly vary from one simulation domain to the other as indicated in TaB. 1. Although the variation does not big influence on computed results, it is pobably caused by adjustment of angle of attack that forced cells to realign themselves automatically.

Table 1. Number of nodes and elements generated

Generated mesh element		$\alpha = 8^0$	$\alpha = 15^0$	$\alpha = 19^0$
No of Nodes		3027030	3029312	3030467
No of elements	**Unstructured tetrahedral**	3056719	3048499	3038876
	Structured Wedges	4897680	4904800	4910160
Total Elements		**7954399**	**7953299**	**7949036**

In solver, computations were performed based on finite volume method via commercial FLUENT v172 version. A steady state pressure based solver with absolute velocity formulation was chosen to combine continuity and momentum equations, which govern the flow in fluid domain. A turbulent model $k-\omega$ SST was incorporated for closure of RANS equations since it is robust and effective near the wall [19]. Dirichlet boundary conditions were specified at inlet and Neumann boundary conditions for outlet. Incoming flow velocity equal to 35m/s with turbulence intensity of 0.03 and turbulence viscosity ratio of 0.1 were specified at inlet. At outlet, pressure was retained as zero gauges Pascal with turbulence properties specified as same as at inlet. The reference fluid flow density in the study was taken equivalent to air density at sea level (1.225kg/m^3) for the fluid with dynamic viscosity of $\mu = 1.462 \cdot 10^{-5} kg/m-s$. No-slip boundary conditions were specified for boundary walls and blade surfaces. The contact region was defined as mesh interfaces with their respective boundaries changed to symmetries.

A Semi-Implicit Method for Pressure-Linked Equation (SIMPLE) algorithm was selected to decouple pressure and velocity in continuity and momentum equations in a segregated manner. The pressure correction equation was solved implicitly while velocity explicitly. Pressure was interpolated using second order discretization scheme. In order to reduce the effects of numerical diffusion, second order upwind spatial discretization scheme was adopted for momentum, diffusion and conservative terms. The convergence criteria solution was monitored through residuals tolerance and coefficient of lift and drag to fall below 10^{-6}. Solution in steady state was achieved after 2000 iterations that resulted to convergence of continuity residual, coefficient of lift and drag coefficient.

3. Results and Discussion

3.1 Verification of fluid domain model

All simulation models were verified by checking the net mass flux flow rate. For all simulations, the flux flow rate obtained fell below -2.0 *10^{-5} kg/s. This is an indication that all simulations were correctly solved and obey continuity law shown in Eq. (1), which state that, for incompressible flow, mass flux flow in must be equal to mass flux flow out assuming fluid flow density remain constant throughout the streams flow.

$$V_{in}A_{in} = V_{out}A_{out} = VA = \text{Constant} \quad (1)$$

Where

V_{in} - velocity at inlet,

V_{out} - velocity at outlet,

A_{in} – inlet area,

A_{out} – outlet area

3.2 Comparison of pressure coefficient at 60%R (RISOE_121 airfoil) for different angles of attack.

Results obtained from CFD computations were compared to experimental measurements for dimensionless coefficient of pressure. The coefficient of pressure can be calculated by given Eq. (2).

$$C_p = \frac{2\left(P - P_{ref}\right)}{\rho_\infty \cdot V_\infty^2} \quad (2)$$

Where P represents absolute pressure over blade's profile, P_{ref} corresponds to static pressure, ρ_∞ free upstream flow density and V_∞ is free upstream flow velocity.

Comparison was done at 60%R and 92%R stations of MEXICO blade, which represent RISOE_121 airfoil section and NACA64-418 airfoil section respectively. Fig. 5 plots comparison results of coefficient of pressure for CFD simulations and experiment measurements performed at 60%R RISOE_121 airfoil section for different angle of attack. This Fig.5 illustrates a good agreement of pressure coefficient distribution on pressure side with slight variation observed for angle of attack $\alpha = 8^0$ between range of $x/c = 0.15$ and $x/c = 0.5$ of the stated airfoil chord. Nevertheless, a big variation is encountered on suction side for different angle of attack within range given as follow: for $\alpha = 8^0 = x/c = 0-0.3$, for $\alpha = 15^0 = x/c = 0.1-0.6$, and for $\alpha = 19^0 = x/c = 0-0.1$. Good agreement is attributed to good flow attachment observed on lower side of the airfoil. In Fig. 5 (a), pressure distribution is slightly underestimated on both sides of airfoil, Fig. 5(b) pressure distribution is overestimated between $x/c = 0.1-0.6$ region on suction side, likewise for Fig. 5(c) between $x/c = 0.15-0.4$. This discrepancy can be attributed to larger twist angle of nearly $\beta = 5.5^0$ or poor mesh quality for the first $x/c = 0.4$ region of leading edge. In order to visualize flow behaviour over the airfoil, the streamlines velocity and pressure contours over the airfoil are displayed on Figs 6 and 7 respectively for 60%R airfoil.

Unfavourable pressure gradient contributes to pronounce of flow separation towards the trailing edge with an increment of angle of attack. Flow separation begins to occur at around 40% chord for $\alpha = 15^0$ and 19^0 and gets more pronounced towards trailing edge. This physical phenomenon is due to adverse pressure gradient that cause eddy flow near trailing edge.

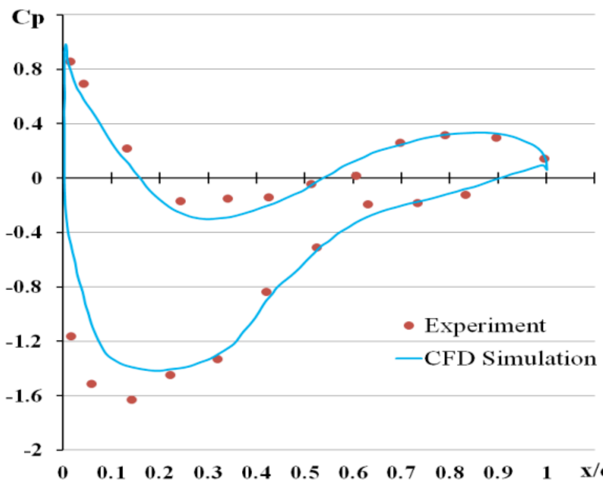

(a)

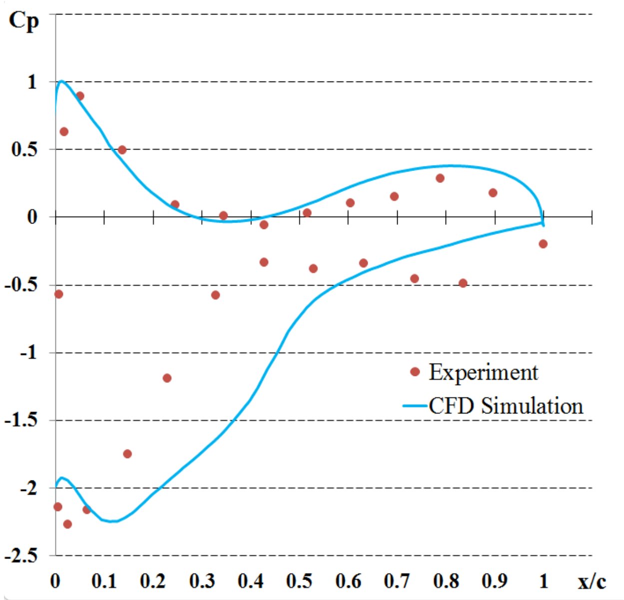

(b)

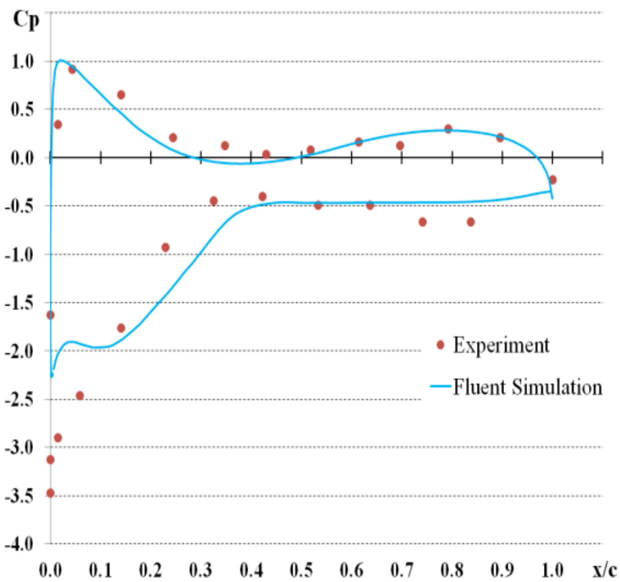

(c)

Fig. 5 Comparison of CFD pressure distribution and experiment measurements for RISOE_121 airfoil (a) at $\alpha = 8^0$ (b) $\alpha = 15^0$ and (c) $\alpha = 19^0$

3.3 Comparison of pressure coefficient at 92%R (NACA64418 airfoil) for different angle of attack.

An excellent agreement to an extent is observed in comparison for computed pressure coefficient and experimental measurements distribution at 92%R (NACA64-418) airfoil section as shown in Fig 8. It is probable that the aerodynamic behaviour is as a result of lower twist angle, small thickness and shape of an airfoil unlike RISOE_121 airfoil.

Fig. 9 and 10, show visualisation of flow behaviour over a NACA64418 airfoil section for given angle of attack; streamlines velocity and pressure contours respectively. The turbulence boundary layer separation begins slightly after leading edge on the upper side while good flow attachment is experienced on lower side. In Fig 9 (b) and (c), curl circulations flow are seen at trailing edge section. This flow phenomenon near trailing edge increases induced drag and it can cause blade to stall due to abrupt drop in lift force.

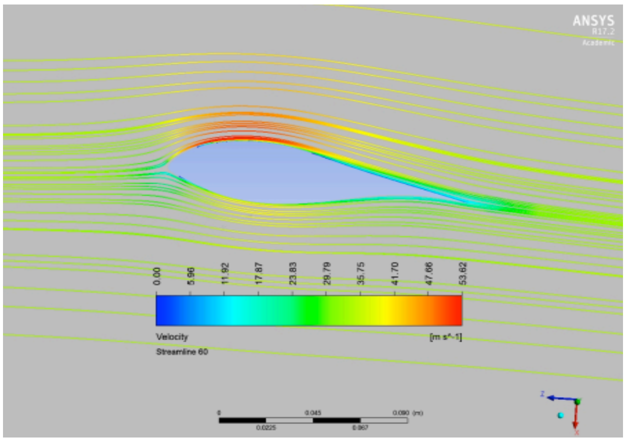

(a)

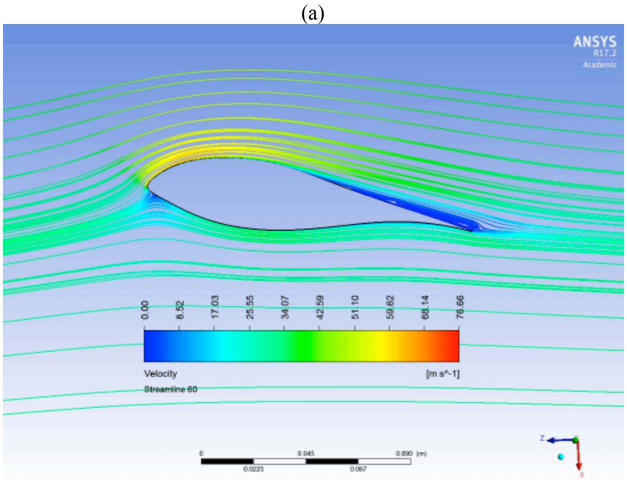

(b)

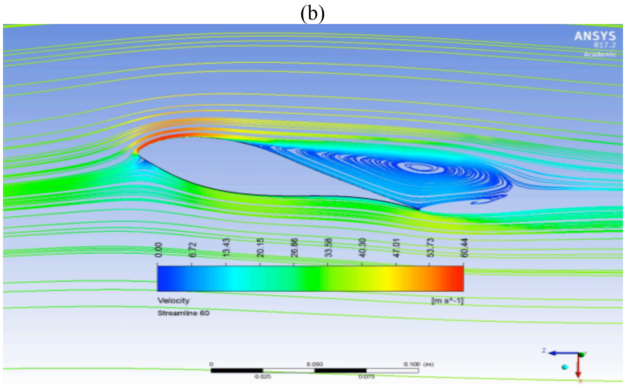

(c)

Fig.6. Velocity vector distribution contours over RISOE_121 airfoil (a) at $\alpha = 8^0$ (b) $\alpha = 15^0$ and (c) $\alpha = 19^0$

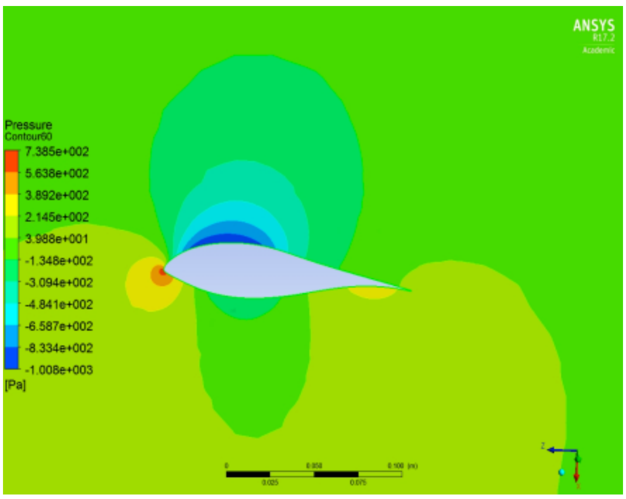

(a)

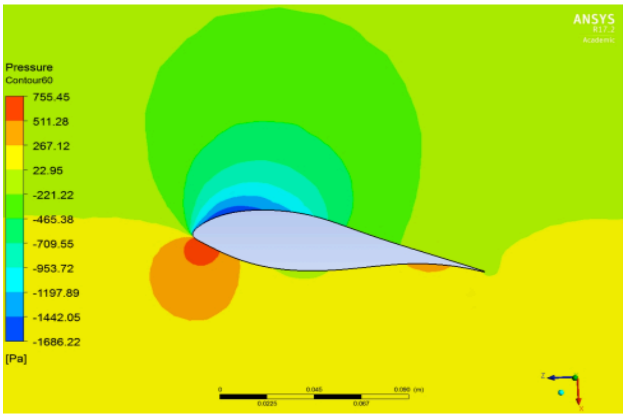

(b)

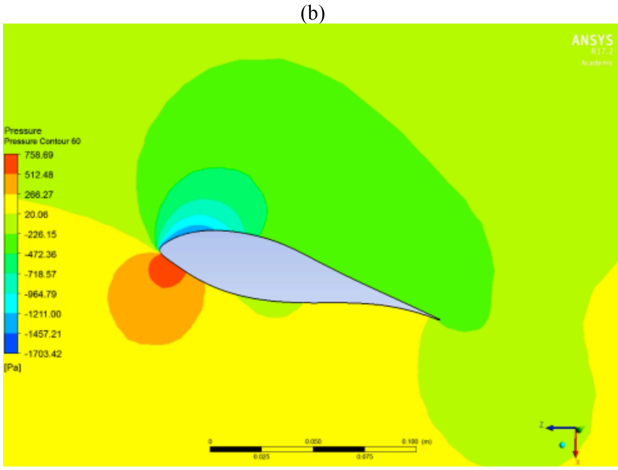

(c)

Fig. 7. Pressure distribution contours over RISOE_121 airfoil (a) at $\alpha = 8^0$ (b) $\alpha = 15^0$ and (c) $\alpha = 19^0$

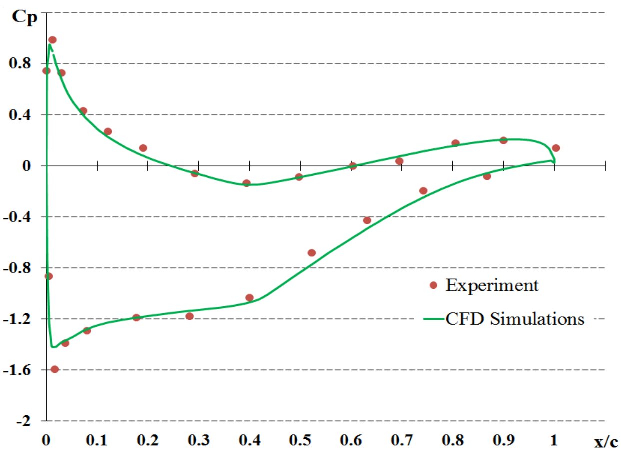

(a)

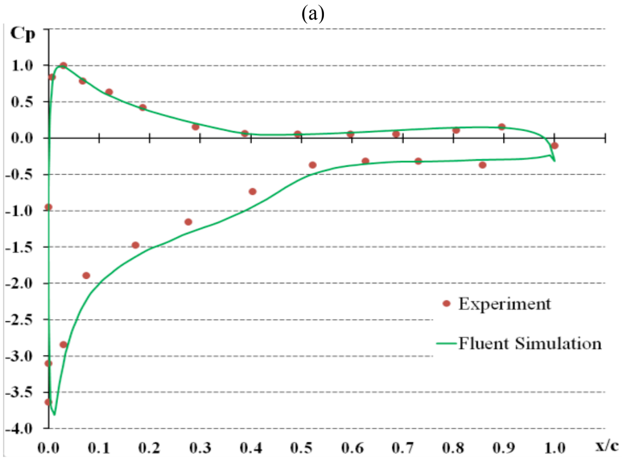

(b)

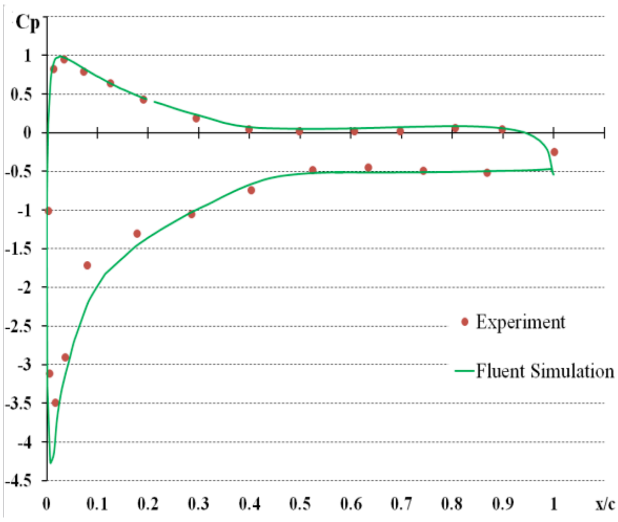

(c)

Fig.8. Comparison of CFD pressure distribution and experiment measurements for RISOE_121 airfoil at (a) $\alpha = 8^0$ (b) 15^0 (c) 19^0

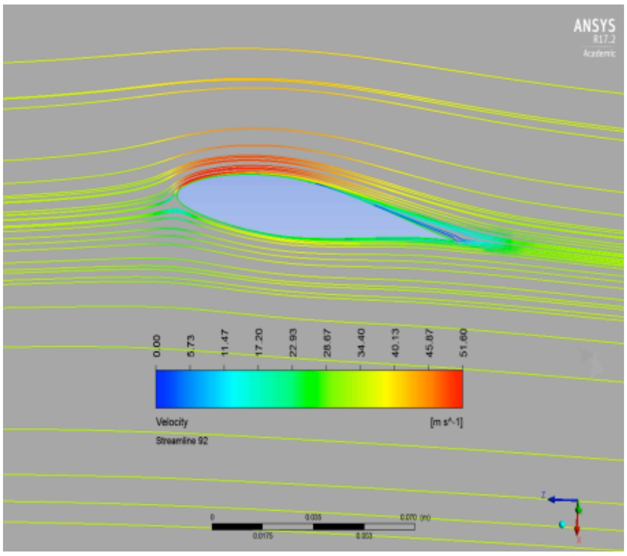

(a)

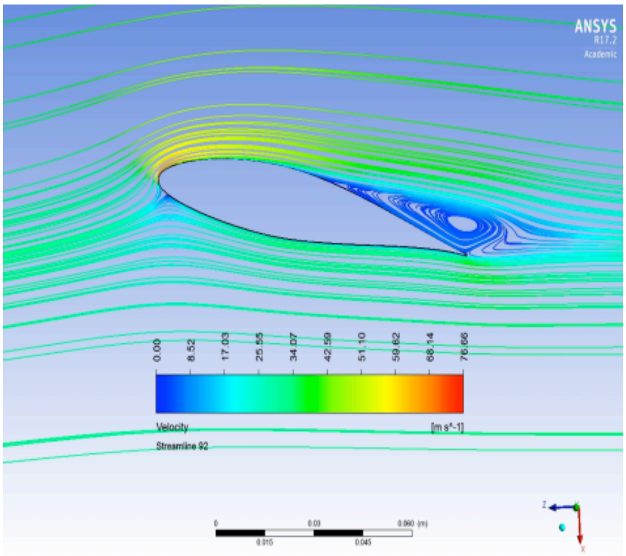

(b)

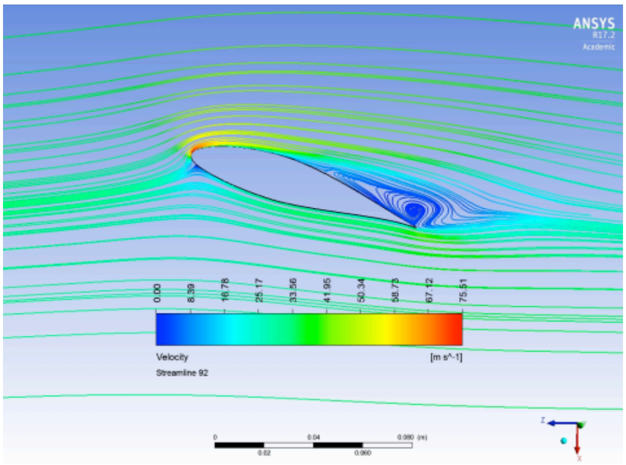

(c)

Fig. 9 Velocity vector distribution contours over RISOE_121 airfoil; (a) $\alpha = 8^0$, (b) $\alpha = 15^0$, (c) $\alpha = 19^0$

Fig. 10 shows pressure contours distribution over NACA64418 airfoil with variation of the angle of attack. Pressure distribution increases with increase in angle of attack.

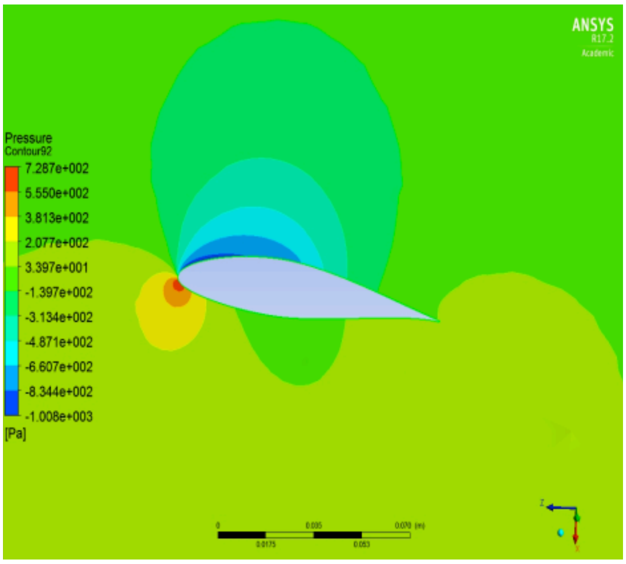

(a)

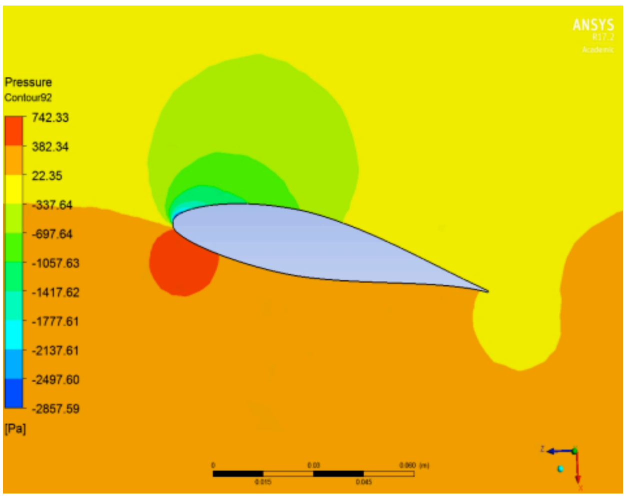

(b)

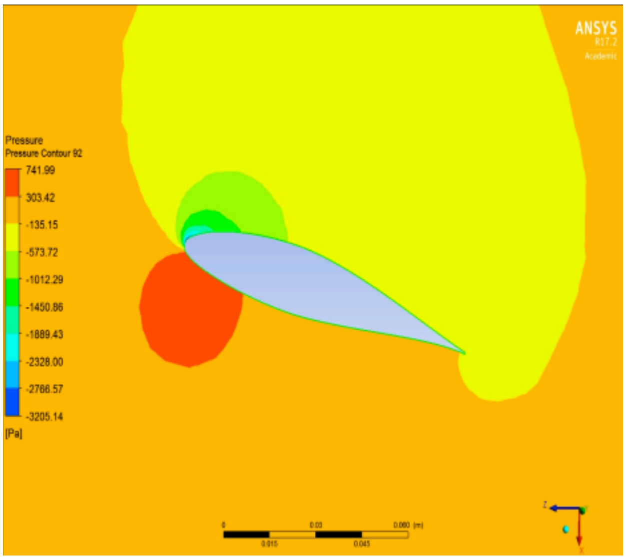

(c)

Fig. 10. Pressure distribution contours over RISOE_121 airfoil for (a) $\alpha = 8^0$, (b) $\alpha = 15^0$, (c) $\alpha = 19^0$

3.4 Comparison of different turbulent model

Further investigation is carried on for simulations using different turbulent models. These include $k-\varepsilon$ Realize turbulent model and Spallat Amalla which are applied separately and then compared with $k-\omega$ SST turbulence model that was initially applied in simulation. In this case, the examination is performed for $\alpha = 15^0$ on RISOE_121 and NACA64-418 airfoil sections. Prediction results are plotted in Fig. 11 (a) and (b) with respect to airfoil section.

In comparison, $k-\omega$ SST appeared more accurate and robust near wall treatment with largely insensitive to the near wall grid resolution. From the result comparison, $k-\varepsilon$ Realizable appeared inappropriate for wind turbine simulation. Slight difference is recorded for $k-\omega$ SST and Sparat Allmaras models. Another sensitive dimensionless variable sensitive to flow over the blade is y+ value. According to Fluent simulations y+ is recommended to lie within $5 < y^+ < 30$ range [20]. In all simulations y^+ variable around the two airfoil sections found to be less than 2.8 as illustrated in Fig 12 (b) and (c).

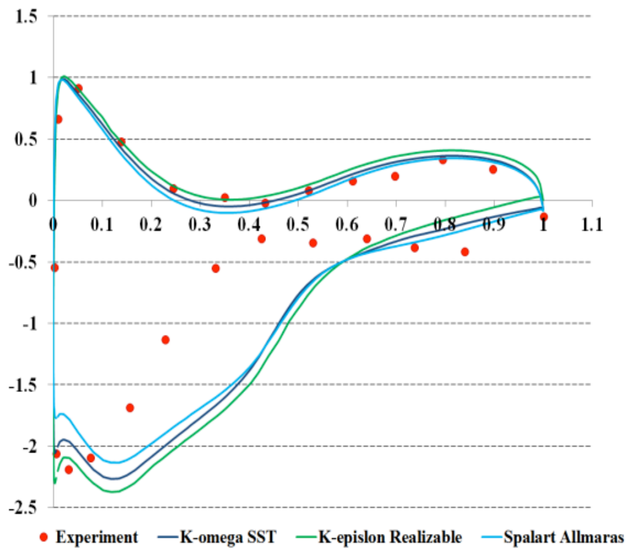

(a)

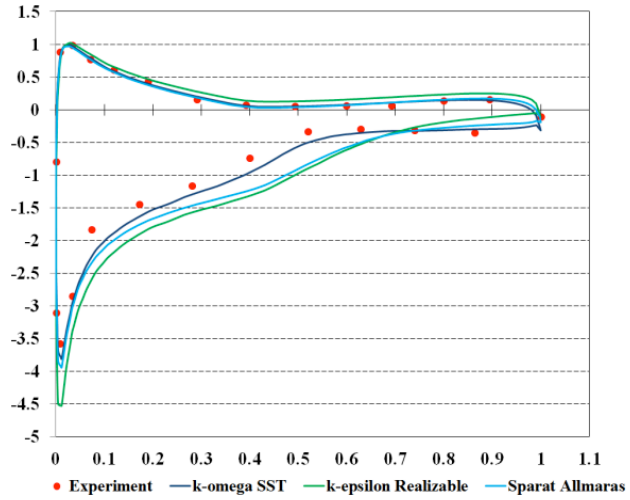

(b)

Fig.11. Comparison of coefficient of pressure for CFD simulation and experiment measurements for different turbulent models for $\alpha = 15^0$ (a) RISOE_121 airfoil section (b) NACA64-418 airfoil section.

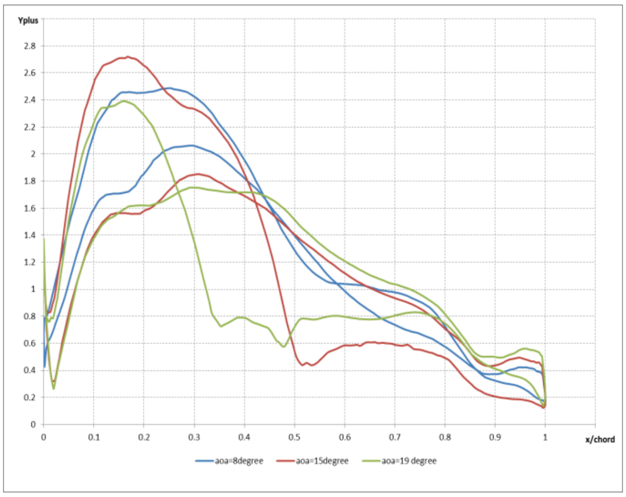

(a)

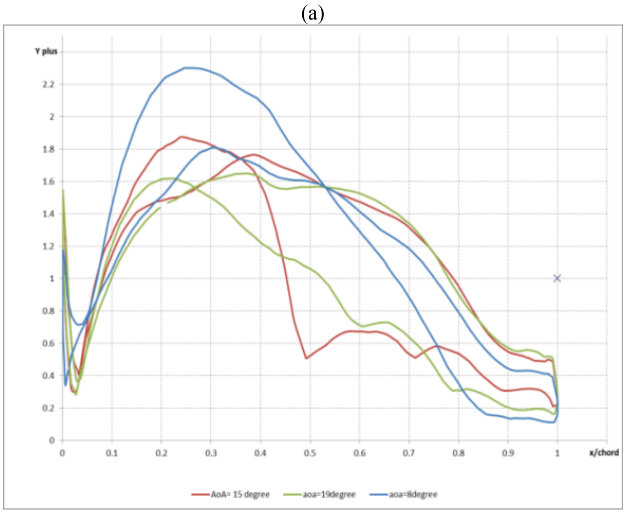

(b)

Fig. 12. Dimensionless y+ distribution for different angle of attack, over; (a) RISOE_121 airfoil, (b) NACA64418 airfoil

The y+ is define $y^+ = yu_\tau / \nu$, where y represent distance from the wall, u_τ is friction velocity, ν is kinematic viscosity and y+ indicates dimension less distance from the wall that is measured in terms of viscous length on the boundary layer. Another agreement variation in comparison would have risen due to twist angle and probable small variation in positioning of blade in wind tunnel or in simulation. The twist angle can influence the angle at which inflow meets with blade, thereby, altering angle of attack.

4. Conclusion

Three-dimensional flow simulations have been performed and compared with wind tunnel experiment measurements. Comparative study shows acceptable agreement of CFD simulations results with experiment measurements. Good comparison agreement is realized for 92%R airfoil section, but huge discrepancy encountered for 60%R airfoil section. For turbulent model, $k-\omega$ SST model is considered appropriate for wind turbine simulations in comparison to $k-\varepsilon$ Realizable and Sparat Allmaras models. The value of y^+ was found less than 5 which is recommended for low Reynolds number flow in FLUENT[20]. However, in order to well capture boundary layer effects, refine mesh near blade surfaces is recommended which was not performed in this study due to limitation of computer processor and physical memory. Another agreement suggests that the pressure coefficient distribution relies heavily on the shape and thickness of the blade and twist angle distribution. The twist angle can influence the angle at which inflow meets with leading edge of the blade, thereby, causing difference inflow behaviour. Possible small variation in positioning of blade either in the wind tunnel or in the simulation domain could also contribute to slight difference in comparison

5. Acknowledgments

The Authors would like to acknowledge that the data used have been supplied by the consortium which carried out the EU FP5 project Mexico: 'Model rotor EXperiments In COntrolled conditions' to which 9 European partners contribute. The Authors are further grateful to acknowledge the financial support from Mobility to Enhance Training of Engineering (METEGA) one of Intra ACP Mobility Schemes through award of a scholarship.

This is an Open Access article distributed under the terms of the Creative Commons Attribution Licence

References

[1] Y. Kumar, J. Ringenberg, S. S. Depuru, V. K. Devabhaktuni, J. W. Lee, E. Nikolaidis, *et al.*, Renewable and Sustainable Energy Reviews **53,** 209-224 (2016).
[2] E. K. Stigka, J. A. Paravantis, and G. K. Mihalakakou, Renewable and Sustainable Energy Reviews **32,** 100-106 (2014).
[3] O. Ellabban, H. Abu-Rub, and F. Blaabjerg, Renewable and Sustainable Energy Reviews **39,** 748-764 (2014).
[4] E. Toklu, Renewable Energy **50,** 456-463 (2013).
[5] A. Evans, V. Strezov, and T. J. Evans, Renewable and sustainable energy reviews **13,** 1082-1088 (2009).
[6] M. Z. Jacobson and M. A. Delucchi, Energy policy **39,** 1154-1169 (2011).
[7] L. Vermeer, J. N. Sørensen, and A. Crespo, Progress in aerospace sciences **39,** 467-510 (2003).
[8] M. S. Siddiqui, A. Rasheed, M. Tabib, and T. Kvamsdal, in Numerical analysis of nrel 5mw wind turbine: A study towards a better understanding of wake characteristic and torque generation mechanism, (IOP Publishing), p. 032059, (2016).
[9] N. Karthikeyan, K. K. Murugavel, S. A. Kumar, and S. Rajakumar, Renewable and Sustainable Energy Reviews **42,** 801-822 (2015).
[10] B. Plaza, R. Bardera, and S. Visiedo, Journal of Wind Engineering and Industrial Aerodynamics **145,** 115-122 (2015).
[11] J. Schepers and H. Snel, ECN Report: ECN-E-07-042 (2007).
[12] H. Snel, G. Schepers, and N. Siccama, in Mexico Project: the database and results of data processing and interpretation, p. 2009-1217, (2009).
[13] M. Carrión, R. Steijl, M. Woodgate, G. Barakos, X. Munduate, and S. Gomez‐Iradi, Wind Energy **18,** 1023-1045 (2015).
[14] L. Oggiano, K. Boorsma, G. Schepers, and M. Kloosterman, in Comparison of simulations on the NewMexico rotor operating in pitch fault conditions, (IOP Publishing), p. 022049, (2016).
[15] C. Tsalicoglou, S. Jafari, N. Chokani, and R. S. Abhari, Journal of Engineering for Gas Turbines and Power **136,** 011202 (2014).
[16] Y. Zhang, A. Van Zuijlen, and G. Van Bussel, in Comparison of CFD simulations to non-rotating MEXICO blades experiment in the LTT wind tunnel of TUDelft, (IOP Publishing), p. 012013, (2014).
[17] J. Schepers, K. Boorsma, T. Cho, S. Gomez-Iradi, P. Schaffarczyk, A. Jeromin, *et al.*, (2012).
[18] P.-E. Réthoré, N. N. Sørensen, F. Zahle, A. Bechmann, and H. A. Madsen, in MEXICO wind tunnel and wind turbine modelled in CFD, (2011).
[19] I. Herraez, W. Medjroubi, B. Stoevesandt, and J. Peinke, in Aerodynamic simulation of the MEXICO rotor, (IOP Publishing), p. 012051, (2014).
[20] https://confluence.cornell.edu